Carbohydrate Polymers 333 (2024) 121981

Contents lists available at ScienceDirect

Carbohydrate Polymers

journal homepage: www.elsevier.com/locate/carbpol

PFAS-free superhydrophobic chitosan coating for fabrics

Irene Tagliaro [a,*], Massimiliano Mariani [a], Raziyeh Akbari [a], Marco Contardi [b,c,d], Maria Summa [e], Francesco Saliu [b], Roberto Nisticò [a], Carlo Antonini [a,*]

[a] Department of Materials Science, University of Milano - Bicocca, via Cozzi 55, 20131 Milano, Italy
[b] Earth and Environmental Science Department, University of Milano-Bicocca, Piazza della Scienza 1, 20126 Milano, Italy
[c] MaRHE Center (Marine Research and High Education Center), Magoodhoo Island, Faafu Atoll 12030, Maldives
[d] Smart Materials, Istituto Italiano di Tecnologia, Via Morego 30, 16163 Genova, Italy
[e] Translational Pharmacology, Istituto Italiano di Tecnologia, Via Morego 30, 16163 Genova, Italy

ARTICLE INFO

Keywords:
Chitosan
Chemical modification
Per- and polyfluoroalkyl substances (PFAS)
Superhydrophobic
Textile coatings

ABSTRACT

In view of health and environmental concerns, together with the upcoming restrictive regulations on *per-* and polyfluoroalkyl substances (PFAS), less impactful materials must be explored for the hydrophobization of surfaces. Polysaccharides, and especially chitosan, are being explored for their desirable properties of film formation and ease of modification. We present a PFAS-free chitosan superhydrophobic coating for textiles deposited through a solvent-free method. By contact angle analysis and drop impact, we observe that the coating imparts hydrophobicity to the fabrics, reaching superhydrophobicty ($\theta_A = 151°$, $\theta_R = 136°$) with increased amount of coating (from 1.6 g/cm^2). This effect is obtained by the combination of chemical water repellency of the modified chitosan and the nano- and micro-roughness, assessed by SEM analysis. We perform a comprehensive study on the durability of the coatings, showing good results especially for acidic soaking where the hydrophobicity is maintained until the 8th cycle of washing. We assess the degradation of the coating by a TGA-IR investigation to define the compounds released with thermal degradation, and we confirm the coating's biodegradability by biochemical oxygen consumption. Finally, we demonstrate its biocompatibility on keratinocytes (HaCaT cell line) and fibroblasts (HFF-1 cell line), confirming that the coating is safe for human skin cells.

1. Introduction

The European Safety Gate, representing the EU rapid alert system for dangerous non-food products, shows that in 2022 35 % of products recalled from the market were banned for chemical risk (European Commission. Directorate-General for Justice and Consumers., 2023). This data highlights that the increased attention to health and environmental protection determined the implementation of more restrictive regulations on chemicals and goods. Thus, non-toxic and biodegradable materials extracted from natural and biotechnological sources, such as chitosan (Iqbal et al., 2023; Petroni et al., 2023; Sreekumar et al., 2022), are becoming increasingly interesting both for science and for industry (Diaz & Crick, 2023). Over the last twenty years, the EU has been applying increasingly restricting regulations on *per-* and polyfluoroalkyl substances (PFAS) that raise concern for their impact on human health (Cathey et al., 2023) and environmental safety. As defined by the Organization for Economic Co-operation and Development (OECD), PFAS are a group of manufactured chemicals which comprises >10,000 molecules. The definition extends to any substance that contains at least one full fluorinated methyl (CF_3-) or methylene (-CF_2-) carbon atom without any H/Cl/Br/I attached. Therefore, the definition for PFAS covers different substances from fluorinated gasses, to polymeric to non-polymeric chemicals.

PFAS are widely used in various sectors such as in food packaging, cosmetics, firefighting foams, electrical products, and especially in clothing and textiles. The actual EU regulation in effect over PFAS has already restricted the use of trimethylsilyl fluorosulfonyldifluoroacetate (TFDA), perfluoroalkyl carboxylic acids (PFCA) and PFCS-related substances under REACH Regulation (EC No. 2021/1297 – Amending Annex XVII to (EC) No.1907/2006) and perfluorooctanoic acid (PFOA), PFOA-related substances and perfluorooctanesulfonic acid (PFOS) under Persistent Organic Pollutants (POP) Regulation (EC No. 2019/1021). For example, the restriction on PFOS defined a limit of 10 mg/kg by weight in substances or mixtures, 0.1 % in articles and 1 μg/cm^2 in textiles and other coated materials. PFOA and its salts are restricted to 0.025 mg/kg by weight in substances, mixtures or articles, PFOA-related

* Corresponding authors.
E-mail addresses: irene.tagliaro@unimib.it (I. Tagliaro), carlo.antonini@unimib.it (C. Antonini).

https://doi.org/10.1016/j.carbpol.2024.121981
Received 28 November 2023; Received in revised form 31 January 2024; Accepted 22 February 2024
Available online 24 February 2024

compounds to 1 mg/kg, while the restrictions on C9 – C14 PFCAs are comparable to that for PFOA.

In February 2023, a new REACH restriction proposal for PFAS was submitted to the European Chemicals Agency (ECHA). This revolutionary proposal will not be focused on one chemical only, as implemented until now, but will concern all PFAS categories. The restriction proposal dossier (Annex XV of REACH-Table 2) defined that, among others, the main application areas include the TULAC (textiles, upholstery, leather, apparel and carpets) areas. The proposal imposes a limit of 25 ppb for any PFAS, 250 ppb for the sum of PFAS, and 50 ppm for polymeric PFAS calculated as total fluorine. The expected time for this regulation to be finalized, after the consultation and evaluation from ECHA, is 2025/2026, with an 18-month window for entry into force after final approval.

Such incoming regulation imposes, especially to the TULAC industries, to find safer and efficient solutions for finding substitutes for PFAS, since PFAS are still the main source of water-repellant chemicals. Silicon-based coatings, mainly comprising silanes and siloxanes, are considered safer alternatives for fabrics (Cai et al., 2018; Chen et al., 2016; Hou et al., 2018; Lahiri et al., 2019; Qi et al., 2022; Zhao et al., 2019; Zhu et al., 2011), but they do not biodegrade and therefore lower the comprehensive environmental sustainability of natural and synthetic fabrics(Mazzon et al., 2021), introducing water wastes depuration problems. Other effective alternatives based on biological raw materials are waxes, which assure non-toxicity and have no environmental concern. Recent studies developed a layer-by-layer deposition method comprising poly-L-lysine and wax deposited for hydrophilizing cotton fabrics (Forsman et al., 2017). A temperature treatment up to 105 °C proved to increase hydrophobicity thanks to the formation of microscopic roughness (Forsman et al., 2020). Besides their proved hydrophobizing effect, they suffer from poor durability and low thermal instability (Fleetwood et al., 2023). Therefore, waxes are usually formulated together with polyurethane, but still have the disadvantage of phase separation and inhomogeneity effects due to the formation of whitish areas when crumpled (Sachan & Purwar, 2022; Saji, 2020). Acrylic resins are also possible alternatives (Wu et al., 2022), but they are known to induce a stiffening in the fabric.

In an effort to mitigate the risks without eliminating PFAS, studies have shown that perfluoropolyethers (PFPE), characterized by repeating units consisting of one to three perfluorinated carbon atoms separated by oxygen atoms in their backbone, could be applied as an alternative to long-chain PFAS (Mohseni et al., 2023).

Other innovative approaches, which still lack industrial validation in the textile field, exploit the hydrophobizing effect of fatty acid aliphatic chains through a complex fabric treatment involving enzyme etching technology with cellulase on cotton fibers, followed by coating with epoxidized soybean oil and further modified with stearic acid (Cheng et al., 2019). In this case, the presence of fatty acids on the surface of the fabric determined the obtainment of water contact angles >150°. The wettability and durability were assessed by static water contact angle, but this method is not as informative as quasi-static measurements, especially when the roll-off performances are crucial and are mainly appreciable by assessing the receding contact angle. Outside the textile application, the hydrophilizing effect of fatty acids has already been exploited for producing antibacterial films (Niemczyk et al., 2019; Vo & Lee, 2017).

In this framework, polysaccharides and especially chitosan-based materials are attracting attention for their low cost and large availability, non-toxicity, and biodegradability (Ladiè et al., 2021). Chitosan-modified products are being widely investigated because of the possibility of tuning their functionality through various chemical reactions (Porpiglia et al., 2024; Sahariah & Másson, 2017) and exploiting their ability to create film (Tagliaro, Musile, et al., 2023), but still have limited application as fabric additives (Raeisi et al., 2021) and are usually proposed as composite materials (Jing et al., 2021; Suryaprabha et al., 2023; Zhang, Liao, et al., 2023; Zhang, Pei, et al., 2023).

In our previous study, we demonstrated the possibility of modifying the chitosan functionality with stearic chains obtaining a PFAS-free superhydrophobic coating on glass substrates thanks to the combinations of low surface energy chemicals with a double-scale morphology (Tagliaro, Seccia, et al., 2023).

Hence, here we investigate the application of the superhydrophobic chitosan-based coating on hydrophobic and hydrophilic fabrics i.g. polyester and cellulose acetate, through a thermal treatment which combines the coating adhesion to the obtainment of surface roughness. This coating is tested in its durability properties showing resistance after washing cycles in acidic pH, and moderate durability for UV-degradation and tear tests. The degradation of the superhydrophobic coating is studied to determine its biodegradability and the specimens formed during degradation, and the coating's biocompatibility is investigated on keratinocytes (HaCaT cell line) and fibroblasts (HFF-1 cell line) The ambition of this study is to pave the way for studying alternative PFAS-free superhydrophobic fabric coatings with limited impact on health and on the environment in view of the upcoming restricting regulations related to fluorinated chemicals.

2. Materials and methods

2.1. Materials

Chitosan powder (DD 80 %, MW 230 kDa, viscosity 330 mPa, CAS 9012-76-4), Stearoyl Chloride (97 %, CAS 112–76-5), Stearic acid (Grade I, ≥98.5 %, CAS 57–11-4), Pyridine (≥99 %, CAS 110–86-1) in analytical grade are purchased from Sigma-Aldrich (Merck-KGaA) and used as received. Dichloromethane (DCM) stabilized with amylene (≥99 %, CAS 75–09-2) is purchased from Thermo Scientific. Ethanol absolute (EtOH) (99 %, CAS 64–17-5) is purchased from VWR Chemicals BDH.

2.2. Superhydrophobic chitosan coating preparation and deposition

Briefly, the modification of 1 g of chitosan is done by esterification and amidation reaction with 13,2 mL of stearoyl chloride in 60 mL of pyridine at 115 °C for 5 h under reflux (Tagliaro, Seccia, et al., 2023). The production is purified by 3 repetitive cycles of dissolution and recrystallization in 100 mL of DCM and 100 mL of EtOH. The product is freeze-dried and sieved over a 100 μm mesh and deposited over cellulose acetate and polyester of 2.5 × 2.5 cm. The fabrics coated with the modified chitosan are treated in the oven at 150 °C to anchor the coating to the fabrics, following a solvent-free coating procedure.

2.3. Methods

The contact angle analysis and the drop impact test are performed using an in-house contact angle setup, consisting of a high-speed camera (Photron Fastcam Nova S6) equipped with a Tokina AT-X PRO D (100 mm F2.8 MACRO) optical lens and a Pump 11 Pico Plus Elite from Harvard Apparatus infusing water through a 30-gauge needle. Positioning the needle close to the surface of interest, water is infused and withdrawn as follows: infusion of 3 μL at a 10 μL/min rate, pause of 3 s, 2nd infusion of 5 μL at a 15 μL/min rate, followed by withdrawal of 10 μL at a 30 μL/min rate. Advancing, θ_A, and receding θ_R, contact angle values are evaluated with DropSnake, a plug-in for ImageJ (Stalder et al., 2006). In this study, surfaces with receding contact angle higher than 135° are defined as superhydrophobic, based on previous experimental (Antonini et al., 2013; Rioboo et al., 2012) and theoretical studies (Li & Amirfazli, 2005).

A dynamic wettability investigation is conducted using drop impact experiments. Accordingly, a liquid droplet is released from a needle installed vertically at various distances from the surface (h) and impacts the samples beneath the needle, resulting in different impact velocities

($U = \sqrt{2gh}$). The liquid evolution after impacting the surface is controlled by the drop kinetic ($\propto \rho U2$) and the surface capillary ($\propto 2\sigma/D_0$) energies, where ρ, σ, and D_0 are the liquid density, the samples' surface tension, and the drop initial diameter, respectively. The ratio of these energies defines the dimensionless Weber number ($We = \rho D_0 U^2/\sigma$) and is used to classify the impact experiment results. In the present study, 5 and 13 μL droplets with initial diameters of $D_0 \sim 2$ *and* 3 *mm*, respectively, freely impact on the samples from h = [0.5, 5] cm distances, i.e. impact velocities U = [0.3, 1] m/s, corresponding to We = [3, 28] in the impact of $D_0 \sim 2$ mm droplets and We = [4, 40] in the impact of $D_0 \sim 3$ mm droplets. The impact videos are recorded using a high-speed camera (Photron Fastcam SA4) with 20 μm px^{-1} spatial resolution, 4 kfps frame rate and at the presence of backlight illumination. All the drop impact experiments are repeated three times to check reproducibility.

Textile surfaces are analyzed by means of Scanning Electron Microscopy (SEM) with a Zeiss Gemini 500 Field-Emission SEM (Carl Zeiss Microscopy, Oberkochen, Germany) at 5 kV. The surfaces have been sputtered with 10 nm gold particles to enhance conductivity.

The coating durability in an acidic environment is tested by submerging the samples for 2 h in a solution of pH 4, rinsing until neutrality with distilled water, and drying for 2 h at 45 °C in the oven. A total of 10 cycles have been performed and contact angle values are measured after each cycle. Adhesion tape test is performed by ISO standard adhesive tape test (EN ISO 2409) using a Scotch Filament tape 8981. The test consists of applying the tape to the sample and gently pressing to obtain a uniform adhesion, before peeling it off. The contact angle is assessed after each cycle, for a total of 5 cycles. Lastly, aging by ultraviolet radiation is performed by RDLAB137 using a QUV Accelerated Weathering Tester QUV/Spray model and applying the irradiation and condensation cycles described in DIN-EN-ISO 4892-3 "Methods for exposing specimens to fluorescent UV radiation, heat and water in apparatus designed to simulate the weathering effects that occur when materials are exposed in actual end-use environments to global solar radiation, or to solar radiation through window glass". More specifically, the samples are exposed to ultraviolet light (340 nm; 0.76 $W \cdot m^{-2} \cdot nm^{-1}$) for 380 h. Each cycle was composed of 10 h with the light on and 2 h with the light off. Applying this condition, during the time the ultraviolet light is off, the temperature of the chamber drops from 60 °C to 50 °C. The relative humidity of the aging chamber is 100 %.

Thermo-gravimetric analysis (TGA) connected with a Fourier-transform infrared spectroscopy (FTIR) system is used to determine the nature of the evolved species during thermal analysis. Samples in powdery form (ca. 20 mg) are placed into an open alumina sample holder, let the weight stabilize for 15 min at 30 °C and heated from 30 °C to 1000 °C (heating rate: 10 °C min^{-1}) under dynamic nitrogen atmosphere (flow rate: 100 cm^3 min^{-1}) by using a Mettler Toledo TGA/DSC1 STARe system. The exhausted gas is piped via a heated transfer line and is continuously analyzed by an FTIR spectrometer during the measurement. FTIR spectra are registered with a Thermo-Fisher Nicolet™ iS20 FTIR spectrometer in the region between 4000 and 600 cm^{-1} (16 scans, 4 cm^{-1} resolution spectra), collecting about 4 spectra per minute, and are analyzed with the OMNIC software (Thermo Fisher Scientific). The IR profiles of reference evolved species are obtained from the National Institute of Standards and Technology (NIST) Chemistry webbook (https://webbook.nist.gov/chemistry/).

Biochemical Oxygen Demand is used to investigate the biodegradability of the samples in the marine environment, which can be easily determined by monitoring the oxygen consumption in a closed respirometer. In detail, about 100 mg of powder material is added to 432 mL of seawater as single carbon source. Seawater is chosen to mimic actual environmental conditions. It already contained microbial consortia and the saline nutrients needed for their growth. The experiment is carried out at room temperature inside dark glass bottles with a volume of 510 mL, hermetically closed with the OxiTop® measuring head. Sodium hydroxide is added as a CO_2 scavenger to sequestrate carbon dioxide produced during biodegradation. Biotic consumption of the oxygen present in the free volume of the system is measured as a function of the decrease in pressure. Samples are tested in triplicate. Raw oxygen consumption data (mg O_2/L) are corrected by subtracting the mean values of the blanks obtained by measuring the seawater's oxygen consumption without any test material. After this subtraction, values are normalized on the mass of the individual samples and referred to 100 mg of material (mg O_2/100 mg material). Finally, the means of the triplicates are calculated and plotted vs. time.

Cytotoxicity assessments are conducted on HaCaT and HFF-1 cells. Specifically, biocompatibility on HaCaT (keratinocytes) is investigated using CellTiter-Glo Luminescent viability assay (Promega Italia S.r.l., Milan, Italy). In 96-well plates, HaCaT cells are placed at a density of 3.5 $\times$ 10^5 in a final medium well volume of 100 μL and incubated until the proper confluence is reached. After 24 h of treatment, cells are quickly rinsed with pre-warmed PBS with Ca^{2+}/Mg^{2+}, and the extraction medium is substituted with the extraction one containing the SCC at different concentrations (0.1, 0.5, 1.0, 2.5, 5.0, and 10.0 mg/mL), while the control samples are treated with medium processed as the extractions. Afterward, cells are incubated for an additional 24 h and 48 h. According to ISO10993-5 guidelines, as the cell viability of the sample extracts is higher than 70 % of the control group, all SCC concentrations are considered biocompatible. Cell viability is determined by measuring ATP levels by CellTiter-Glo assay, as indicated by the supplier as percentage survival relative to control cells. Data are represented as mean ± standard deviation of three independent experiments. The impact of SCC on cell morphology has been also monitored using a LEICA DMI6000B inverted microscope. Likewise, HFF-1 cells are cultured in the same condition and placed at the density of 3.5 $\times$ 10^5 in a final medium well volume of 100 μL. SCC is tested at the concentrations of 0.1, 0.5, 1.0, 2.5, 5.0, and 10.0 mg/mL.

3. Results and discussion

Two different fabrics with different wettability properties, i.e. cellulose acetate and polyester, have been coated with the superhydrophobic chitosan coating. By the naked eye (Fig. 1a and b), the coating deposition on both fabrics looks uniform and results in an extremely repellent surface to various liquids. Water, coffee, orange juice and a methylene blue solution do not wet the coated surface and show high mobility on the surface (Fig. 1a and b).

Different amounts of coatings from 0.8 to 3.2 mg/cm^2 have been deposited over the two fabrics for comparing the wetting properties (Fig. 1c and d). Bare cellulose acetate is a highly hydrophilic material and, therefore, it adsorbs water when in contact with a drop. The deposition of 0.8 mg/cm^2 alters its wettability conferring hydrophobic properties with $\theta_A = 150°$ for and $\theta_R = 125°$. Increasing the amount of the coating to 1.6 and 3.2 mg/cm^2 results in an increase of θ_R to 136° and 133°, close to the limit of 135° used to define the surfaces as superhydrophobic. For the samples 1.6 and 3.2 mg/cm^2, the reduction of hysteresis and of the standard deviation are macroscopic manifestations of coating homogeneity. Polyester is inherently hydrophobic, but not superhydrophobic, with of $\theta_A = 149°$ and $\theta_R = 91°$. The deposition of the coating determines an increase of both θ_A and θ_R to 155° and 139°, respectively, for 0.8 mg/cm^2 resulting in superhydrophobicity. A higher amount of coating does influence the θ_A significantly (153° for 1.6 mg/cm^2 and 159° for 3.2 mg/cm^2), and leads to a slight increase of θ_R for 3.2 mg/cm^2 to 143°.

As such, for both cellulose acetate and polyester, superhydrophobicity is obtained for the deposition of 1.6 mg/cm^2 which from now on we will define as superhydrophobic chitosan coating (SCC).

The hydrophobizing effect of the SCC has been also tested on cotton (Fig. S1), proving the coating efficiency also on very hydrophilic substrates.

The coated and uncoated fabrics with 1.6 mg/cm^2 (SCC) have been

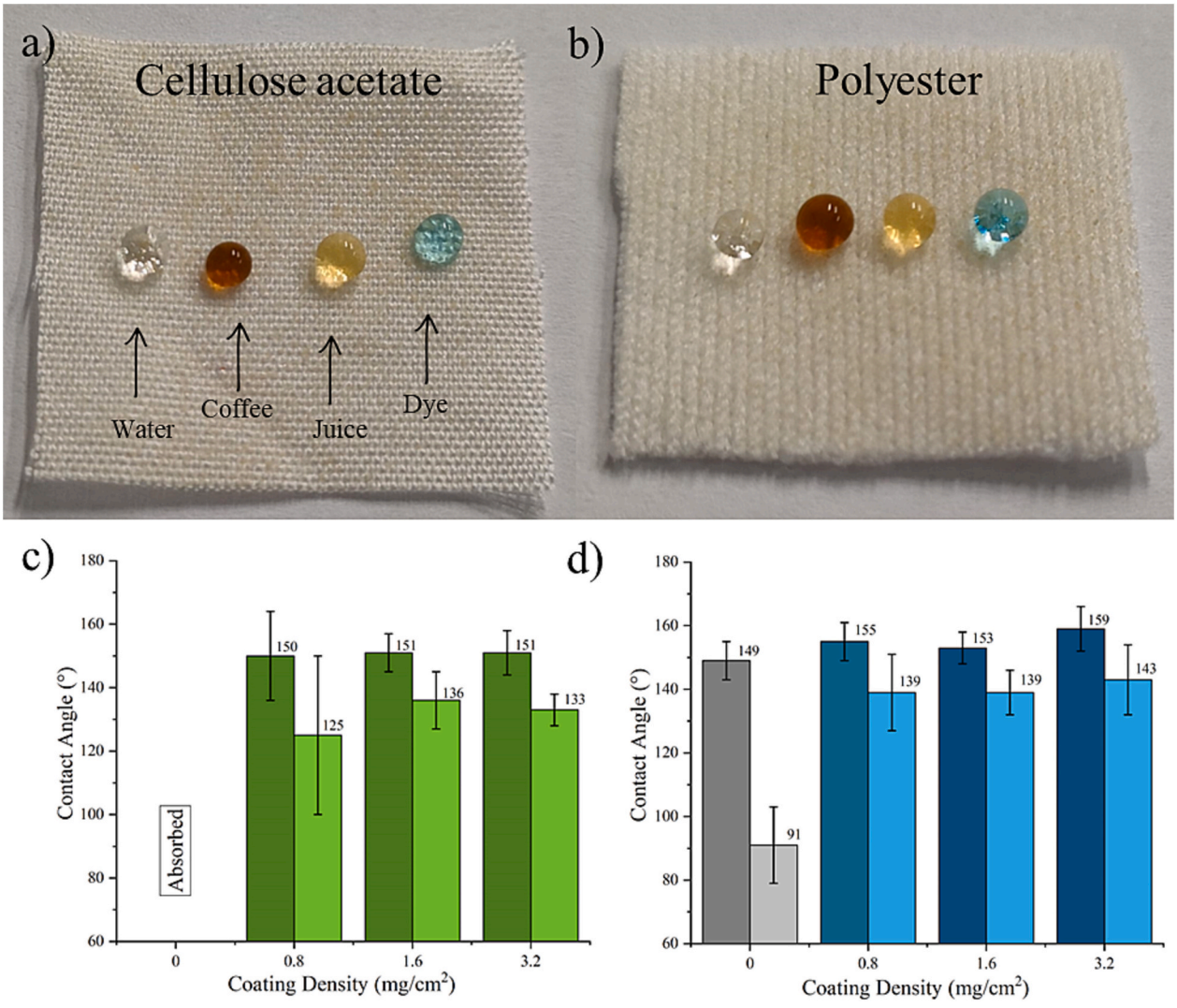

Fig. 1. Pictures of a drop deposited on fabrics of (from left to right) water, coffee, orange juice and a solution of methylene blue (a) on coated cellulose acetate; (b) on coated polyester; quasi-static contact angle analysis on increasing SC on c) cellulose acetate (dark green θ_A, light green θ_R), d) polyester (blue θ_A, light blu θ_R, for coated fabrics; dark gray θ_A, light gray θ_R, for uncoated fabrics).

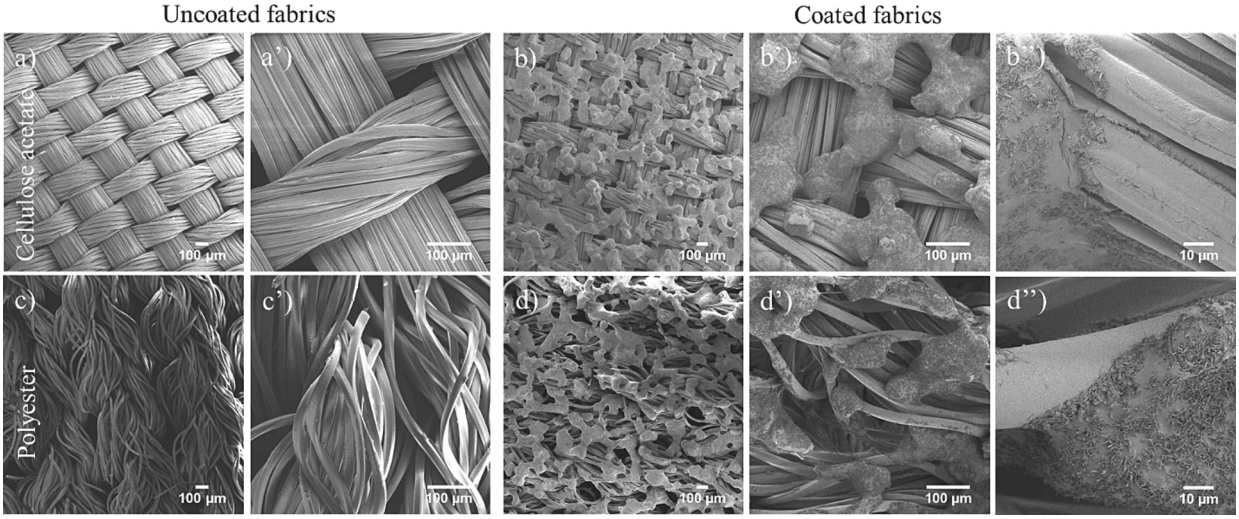

Fig. 2. SEM analysis of coated and non-coated fabrics at three different magnifications: a) uncoated cellulose acetate 100×, a') uncoated cellulose acetate 350×, b) coated cellulose acetate 100×, b') coated cellulose acetate 350×, b") coated cellulose acetate 2500×, c) uncoated polyester 100×, c') uncoated polyester 350×, d) coated polyester 100×, d') coated polyester 350×., d") coated polyester 2500×.

analyzed by SEM to assess the morphology of the coating. Fig. 2a, a' and c, c' shows the uncoated cellulose acetate and polyester, while Fig. 2b, b', b" and d, d', d" the coated fabrics. The coating consists of discrete spots (Fig. 2b and d) that are anchored over the fibers. The spots are ca. 100 μm, which are compatible with the size of the mesh used for deposition (Fig. 2b' and d') and have merged borders. At higher magnification (Fig. 2b" and d") it is possible to appreciate nanometric features which are typical structures of freeze-dried chitosan. The fibers are not entirely coated, but rather covered with discrete separate islands of coating: this observation is similar to other studies using perfluorinated substances (Mohseni et al., 2023)and consistent with the results from contact angle analysis (Fig. 1c and d): with lower chitosan amount, the exposed area of uncoated fabrics is higher and results in higher pinning of drops, with higher standard deviation in both cases of cellulose acetate and polyester. Moreover, high values of θ_A are probably due to the double-size roughness of the coating, which shows micrometric and nanometric roughness, achieving superhydrophobicity. An additional benefit of this deposition method is that the spot-like coating does not result in clogging the fibers' pores, thus maintaining the original breathability of the fabrics.

Referring to Fig. 3a, the impact of the water drop on the surface leads to a complete rebound outcome across all the samples at lower Weber numbers, in alignment with our expectations due to the high receding contact angle (>130°) and minimal wetting hysteresis (< 20°) observed in all the samples, see Fig. 1c and d. Briefly, when a droplet impacts on a superhydrophobic surface, a sudden surge in pressure at the point of impact causes the liquid droplet to deform and swiftly expand outward, assuming a thin disk-like shape. Subsequently, surface tension forces act in opposition to the outward spreading of the liquid drop, particularly at its outer edges, forming what is known as a 'rim'. As the central region of the liquid disk continues to supply liquid to the rim, the accumulated energy and mass within the rim generate an inward pressure once the droplet attains its maximum spread on the surface. The internal pressure drives the rim toward the center of the liquid disk, initiating the recoil phase, during which the solid-liquid contact area rapidly contracts. Subsequently, a vertical jet of liquid emerges from the surface, and this phenomenon can evolve into a complete detachment of the droplet from the superhydrophobic surface, known as a "full rebound" (Mao et al., 1997). Based on the outlined phenomena and Fig. 3a, as Weber number, and thus the drop velocity, increases, a transition is evident in the recoil map, shifting from full rebound to partial rebound, and ultimately culminating in a sticky deposition outcome. This transition signifies that the wetting state of the surfaces begins in the Cassie-Baxter state at very low *We*, and as the *We* number increases, it transits to the Wenzel state. Hence, the liquid can penetrate the surface pores and get trapped inside and causing a delay or prevention in the liquid detachment from the surface; the higher the drop kinetic energy, the higher the penetration to the surface. The high surface roughness combined with the irregular surface coating and the presence of tiny fibers on the surface aim this transition. Despite the increased receding contact angle and drop volume, the recoil phase map exhibited non-uniform characteristics. This variation can be attributed to the inherent non-homogeneity and deformability of the coated fabrics. Notwithstanding these variations, the consistent occurrence of full or partial droplet rebounds on the coated fabrics suggests their ability to maintain effective water repellency under a moderate rainfall (Montero-Martínez & García-García, 2016)(i.e. <0.5 mm rain drops in <2 m/s).

Fig. 3b illustrates the non-dimensional maximum spreading diameter of a droplet on the surface after impact. Based on the previous findings, the ratio between the maximum spreading diameter on the solid surface to the drop initial diameter, D_{max}/D_0, at low Weber numbers is proportional to a power of *We*. This relationship is approved by both the energy-based models and the experimental correlation (Antonini et al., 2012). The data in Fig. 3b can be effectively fitted with a power exponent of 0.2, consistent with earlier findings, such as those reported by Clanet et al. (2004).

An extensive evaluation of the SCC durability has been performed for assessing the wettability properties after repeated cycles in different harsh environments. The durability is tested for soaking fabrics at pH 4 for 10 cycles, for UV aging for >300 h and for standard tape test EN ISO 2409 for 5 cycles (Fig. 4a). For the test in acidic water, coated cellulose acetate (Fig. 4b) shows no great fluctuation of θ_A and θ_R over the first 8 cycles with values oscillating respectively around 150° and 136°. After the 9th cycle, θ_R drops to 119°. Polyester (Fig. 4c) also shows no significative reduction of contact angle values until the 10th cycle where θ_A is 145° and θ_R is 130°. The contact angle analysis for soaking cycles demonstrates excellent durability to repeated submersion at acidic pH, with reduction of performances only after 9 cycles for cellulose acetate and 10 cycles for polyester. This test suggests that the coating would be resistant to repeated washing cycles and to acidic rain exposure.

Standard condition described in the DIN-EN-ISO 4892-3 have been selected for assessing durability to UV aging, for mimicking the effect of

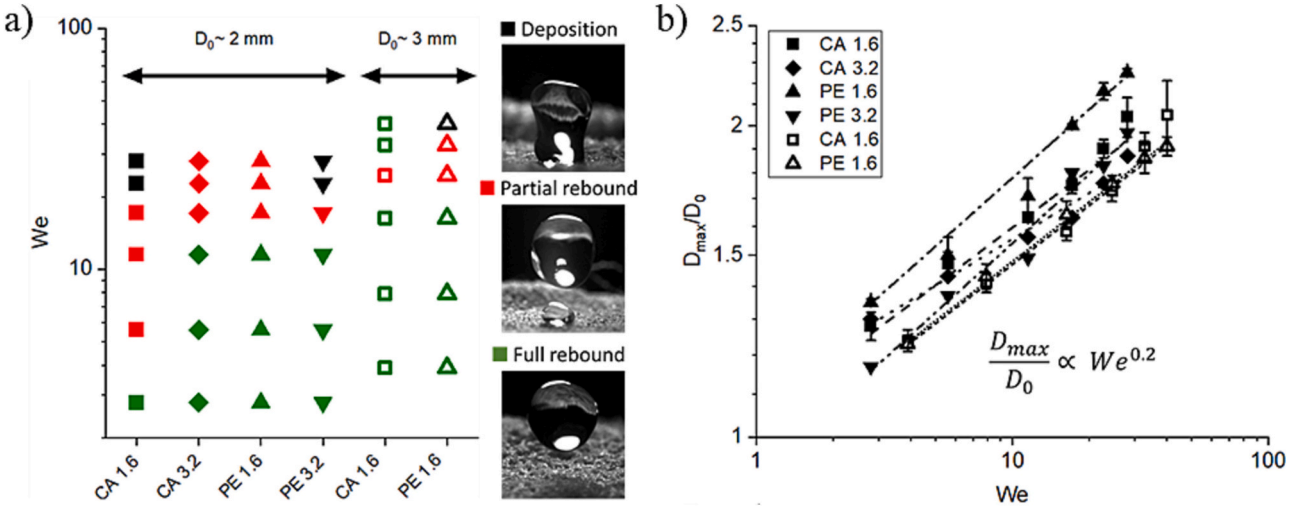

Fig. 3. Drop impact investigation of the coated cellulose acetate and polyester fabrics. 'CA 1.6', 'CA 3.2', 'PE 1.6', and 'PE 3.2' legends refers to the results from the impact of a 5 μL distilled water droplet ($D_0 \sim 2$ *mm*) on the corresponding samples. To study on the effect of the impacting droplet on the impact outcomes, two sets of the drop impact studies performed on CA 1.6 and PE 1.6 samples with 13 μL droplet ($D_0 \sim 3$ *mm*), presented in the figure with hollow symbols. a) Drop impact outcomes during recoil above the samples. Images from different recoil outcomes observed above the fabric presented in the right side of the graph. b) A ratio of the maximum droplet diameter on the surface and the initial droplet diameter before impact vs. We.

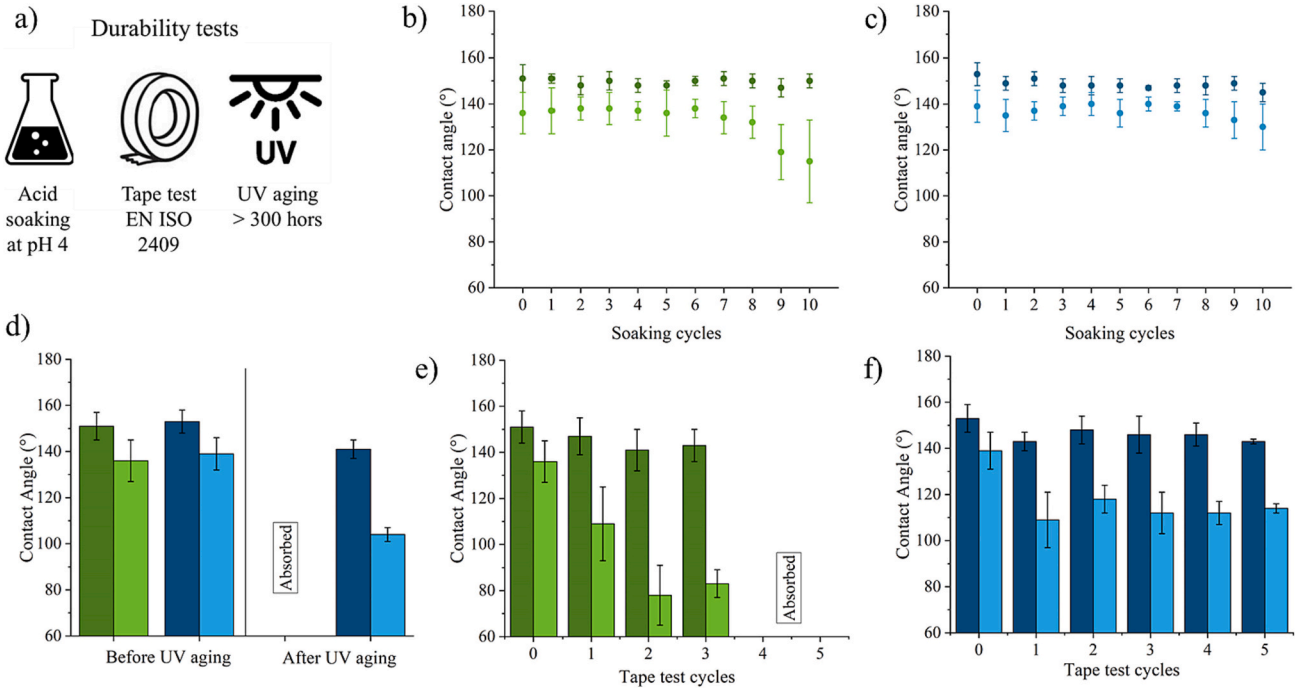

Fig. 4. a) Scheme of durability tests; durability test for acid soaking at pH 4 for b) cellulose acetate and c) polyester; d) durability under UV aging; durability for tape test EN ISO 2409 e) cellulose acetate and f) polyester.

intensive exposure to the sun and high humidity. The total UV dose applied is estimated by using the tester bolometer of the chamber and resulted 170 MJ m^{-2} which roughly corresponds to 10 months of outdoor exposure at 31° N latitude. Fig. 4d shows the wettability properties before and after the intensive UV treatment. Cellulose acetate adsorbs water after the test, while polyester lowers to θ_A of 141° and θ_R of 104°, similar value to non-coated fabrics. The UV aging test results in a degradation of the coating performances to the ones of bare fabrics.

The standard test EN ISO 2409 has been performed to assess the coating adhesion and to ensure resistance to the abrasive stress. Cellulose acetate (Fig. 4e) shows a decrease of θ_A and θ_R after the first cycles to 147° and 109°, with the adsorption of the water at the 4th cycle. Similarly, polyester (Fig. 4f) shows a decrease of θ_A and θ_R already after the first cycle to 143° and 109°, respectively, reaching a plateau until the 5th cycle. The tape test results in a considerable degradation of the wetting performance of the coating. The weak bonds, which enable the coating adhesion to the fabrics, are not strong enough to endure tears of adhesive tapes and determine the coating removal.

TGA under a dynamic nitrogen atmosphere has been coupled with FTIR spectroscopy to study the products of the thermal degradation. Fig. 5a shows the thermal profiles of the SCC, compared with the reference chitosan, stearoyl chloride, and stearic acid. In detail, bare chitosan exhibits an overall weight loss of ca. 68.4 wt%, with two main degradation steps, the first one at temperature below 150 °C attributable to physically-sorbed water (moisture, ca. 8.9 wt%), followed by the main relevant one at a temperature higher than 300 °C with a long tail corresponding to a complex degradation pathway (Corazzari et al., 2015). Stearoyl chloride, instead, exhibited an overall weight loss of ca. 93.2 wt%, with two mass losses, the main relevant one at a temperature higher than 250 °C (very steep profile) followed by a second one (slower) at a temperature higher than 300 °C, reaching a plateau at ca. 500 °C. Interestingly, bare stearic acid displayed an overall weight loss of ca. 94.1 wt%, with a single mass loss at a temperature higher than 250 °C (very steep profile) due to the stearic acid evaporation (Y. Chen et al., 2017), and leaving at 1000 °C a solid residue of ca. 5.6 wt%. Lastly, the thermogram of the SCC shows an intermediate behavior between pristine chitosan and stearic species, exhibiting a single mass loss starting at a temperature higher than ca. 250 °C, reaching a plateau at ca. 500 °C, and leaving at 1000 °C a solid residue of ca. 9.9 wt%. Fig. 5b shows the Gram-Schmidt plots of both pristine chitosan, and SCC. In particular, with this information, it is possible to determine the time and temperature at which the major decomposition events occurs, namely at around 44 min (corresponding to ca. 300 °C), whereas Fig. 5c and Figure 5dD reported the IR spectra of evolved species produced during this step for both pristine chitosan and SCC, respectively. In particular, the IR spectrum of the volatile species deriving from the pyrolysis of pristine chitosan (Fig. 5c) evidences the presence of the characteristic IR signals of H_2O, CO_2, CO, and acetic acid, with absence of NH_3 ones (Corazzari et al., 2015). According to Corazzari et al., it has been demonstrated that the fate of the amino groups deriving from the glucosamine structure forming the chitosan chains can be twofold, namely: (i) ammonia release, and (ii) heteroaromatic rings formation (mostly entrapped in the solid residue) (Nisticò et al., 2020). In the case of the degradation profile of SCC (Fig. 5d), instead, the IR characterization of the evolved gas released during the pyrolysis clearly evidences the contribution due to stearic acid, thus confirming the presence of the functionalizing agent in the sample. Due to the large contribution of the evolved stearic acid and the low intensity of the volatiles coming from the chitosan pyrolysis, the chitosan contribution is completely covered (i.e., the variation of the H_2O and CO_2 IR signals registered in the spectrum is negligible and can be associated to the atmosphere rebalancing) and cannot be quantified.

Biochemical oxygen consumption test has been performed to evaluate the biodegradability of the new coating. Fig. 6 reports the oxygen consumption for the SC, microcrystalline cellulose as positive control, and polypropylene as negative control. After 4 days, degradation of the SC and microcrystalline cellulose starts and, after 30 days, 9 and 14 mg O_2/100 mg have been consumed, respectively. Differently, polypropylene does not show any signal of biodegradation during the entire period of analysis. These results confirm that the introduced stearoyl modification of chitosan does not alter its biodegradable nature. Thus, such SCC can be utilized for fabrics but also other applications without impacting the environment and addressing the United Nations' Sustainable Development Goal 12 (SDG 12), which requires the

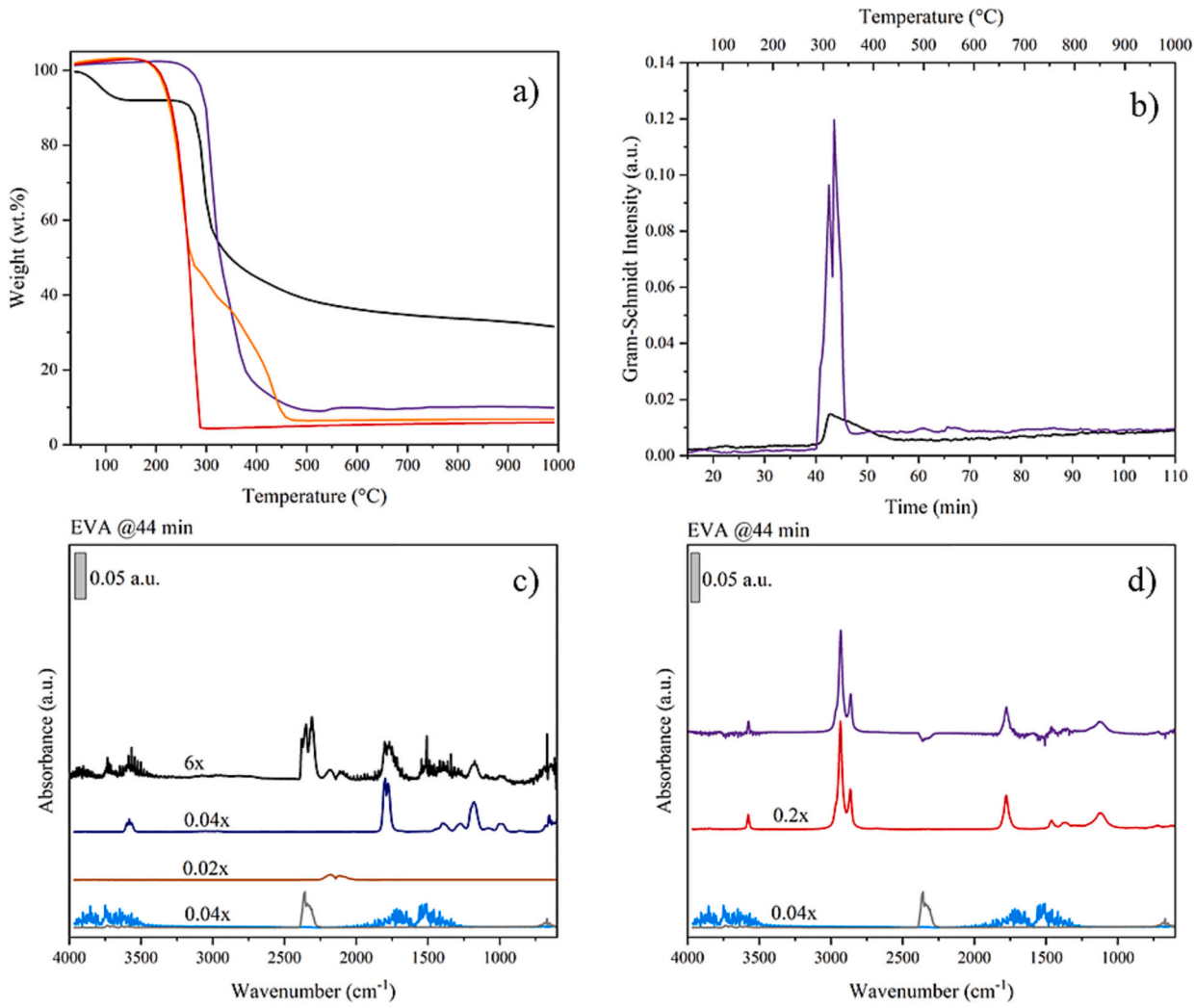

Fig. 5. a) TGA curves of: SCC (purple), pristine chitosan (black), stearoyl chloride (orange), and stearic acid (red) under dynamic nitrogen atmosphere; b) Gram-Schmidt plots of evolved species release from SCC (purple), and pristine chitosan (black), during the heating ramp expressed as a function of the temperature and time; c) FTIR spectrum of volatiles released during heating ramp (sampled after 44 min) of pristine chitosan (black), compared with the reference FTIR spectra of H_2O (light blue), CO_2 (gray), CO (brown), and acetic acid (navy blue); d) FTIR spectrum of volatiles released during heating ramp (sampled after 44 min) of SCC (purple), compared with the reference FTIR spectra of H_2O (light blue), CO_2 (gray), and stearic acid (red).

introduction of new material with a well-kwon life cycle also after their discard (Adeboye et al., 2023).

Finally, the biocompatibility of the superhydrophobic chitosan has been tested on keratinocytes (HaCaT) and fibroblasts (HFF-1) (Fig. 7). The viability after 24 and 48 h of exposition to the SCC at different concentrations resulted in being above 70 % and thus according the ISO10993-5 guidelines can be defined biocompatible for both the used cell lines. These results are further confirmed by morphological analysis (Figs. S2 and S3). Both keratinocytes and fibroblasts did not change their shapes or showed any signal of toxicity, confirming that SCC is biocompatible and non-toxic for human skin cells.

4. Conclusion

A PFAS-free superhydrophobic coating has been produced and deposited by a solventless approach to fabrics with opposite wettability properties namely cellulose acetate (hydrophilic) and polyester (hydrophobic). Both coated fabrics show superhydrophobicity by applying only 1.6 mg/cm^2 of coating, reaching quasi-static contact angles of $\theta_A = 151^\circ$ and $\theta_R = 136^\circ$ in the case of cellulose acetate, and $\theta_A = 153^\circ$ and $\theta_R = 139^\circ$ in the case of polyester. SCC demonstrated a full rebound response to drop impacts adequate to protect fabrics under moderate rainfall. The morphology of the deposited coating has been characterized by SEM identifying the formation of a spot-like coating with covered areas of ~100 μm and roughness at the nanometric scale. The morphological characteristics are in agreement with the obtainment of superhydrophobicity and with the drop impact behavior.

Durability tests have been performed on SCC for assessing the coating resistance under harsh environments such as soaking in acidic water (pH 4), UV exposure and tape standard tests. The coating shows excellent resistance on both fabrics for cycles of acidic soaking with no significative variations of contact angles until the 8th cycle for cellulose acetate and until the 10th cycle for polyester. Extremely harsh conditions of UV exposure tests, corresponding to 10 months of outdoor exposure at 31° N latitude, results instead in the degradation of the coating on both fabrics. Standard tape tests show moderate coating resistance after the first tear but result in the removal of the coating after multiple tears.

By TGA-FTIR characterization of the SCC thermal decomposition, we can appreciate the evolved gas released during the pyrolysis which clearly evidences the contribution due to stearic acid with the effect of hiding the signals typical of chitosan of H_2O, CO_2, and CO. By biochemical oxygen consumption test, we have verified the effective biodegradability of the coating which confirms that the introduction of

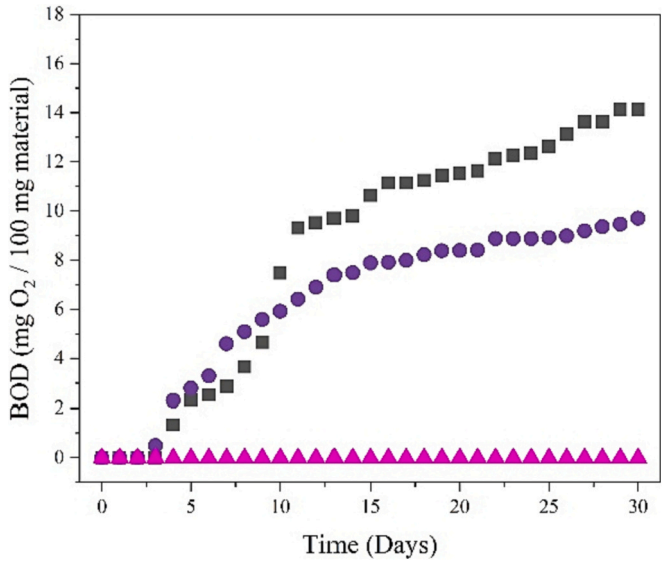

Fig. 6. Biochemical oxygen consumption (mg O_2/100 g material) as a function of time (days) for the microcrystalline cellulose (black squares), SC (purple circles), and polypropylene samples (pink triangles).

stearoyl modification does not alter its biodegradable nature. Finally, we demonstrate the excellent biocompatibility of the SCC on human keratinocytes and fibroblasts, enabling safe contact with the skin.

While the functionality modification of chitosan involves the use of solvents that are not environmentally friendly (specifically pyridine, a hard-to-replace solvent as an acid scavenger in reactions with acyl chlorides, and dichloromethane during the purification), the solventless deposition method adheres to environmental sustainability requirements. This approach limits the use of solvents during the chitosan modification step and eliminates the need for end-users to handle solvents. Our future objective is to improve the reaction toward environmentally friendly solvents.

CRediT authorship contribution statement

Irene Tagliaro: Writing – review & editing, Writing – original draft, Supervision, Investigation, Formal analysis, Conceptualization. **Massimiliano Mariani:** Investigation, Formal analysis. **Raziyeh Akbari:** Writing – review & editing, Investigation, Formal analysis. **Marco Contardi:** Writing – review & editing, Investigation, Formal analysis. **Maria Summa:** Investigation. **Francesco Saliu:** Writing – review & editing, Investigation, Formal analysis. **Roberto Nisticò:** Writing – review & editing, Investigation, Formal analysis. **Carlo Antonini:** Writing – review & editing, Supervision, Methodology, Funding acquisition, Conceptualization.

Declaration of competing interest

The authors declare that they have no known competing financial interests or personal relationships that could have appeared to influence the work reported in this paper.

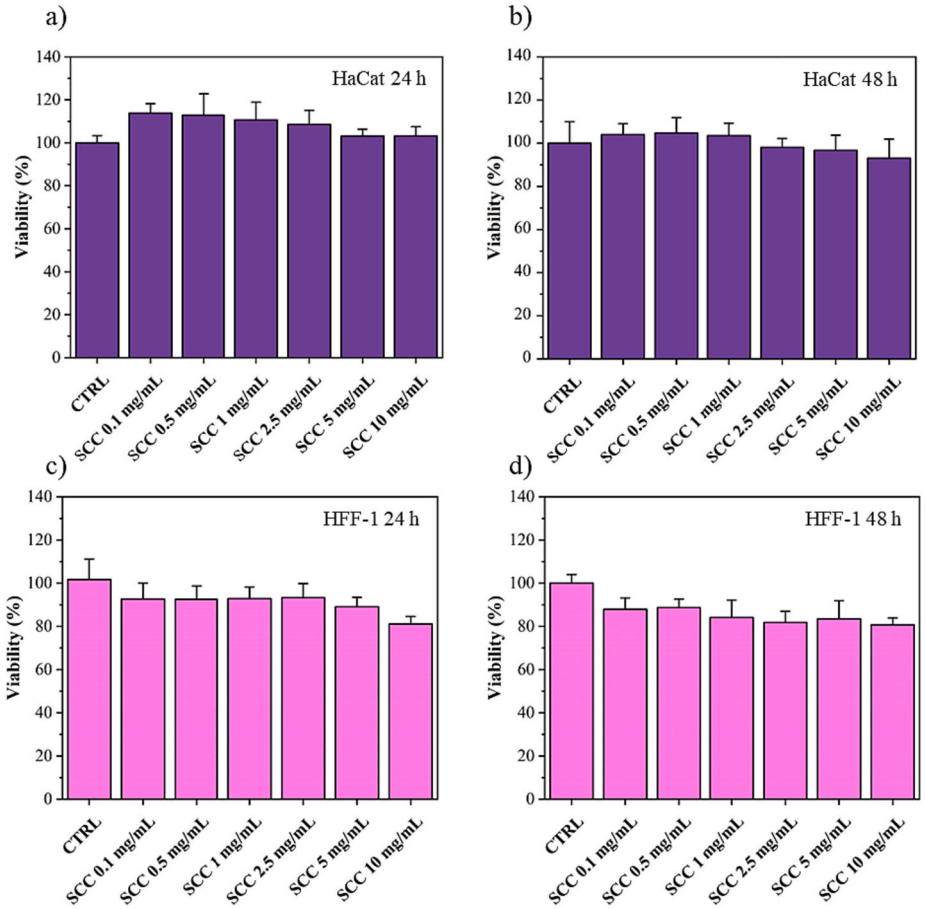

Fig. 7. Histogram of cell viability HaCaT cells for the control, SCC 0.1, 0.5, 1.0, 2.5, 5.0, 10.0 and mg/mL, (purple bars) after a) 24 and b) 48 h; histogram of cell viability on HFF-1 cells for the control, SCC 0.1, 0.5, 1.0, 2.5, 5.0, 10.0 and mg/mL, (pink bars) after a) 24 and b) 48 h.

Data availability

Data will be made available on request.

Acknowledgments

This research received no external funding.

Appendix A. Supplementary data

Supplementary data to this article can be found online at https://doi.org/10.1016/j.carbpol.2024.121981.

References

Adeboye, S. A., Adebowale, A. D., Siyanbola, T. O., & Ajanaku, K. O. (2023). Coatings and the environment: A review of problems, progress and prospects. *IOP Conference Series: Earth and Environmental Science, 1197*(1). https://doi.org/10.1088/1755-1315/1197/1/012012

Antonini, C., Amirfazli, A., & Marengo, M. (2012). Drop impact and wettability: From hydrophilic to superhydrophobic surfaces. *Physics of Fluids, 24*(10). https://doi.org/10.1063/1.4757122

Antonini, C., Villa, F., Bernagozzi, I., Amirfazli, A., & Marengo, M. (2013). Drop rebound after impact: The role of the receding contact angle. *Langmuir, 29*(52), 16045–16050. https://doi.org/10.1021/la4012372

Cai, R., Glinel, K., De Smet, D., Vanneste, M., Mannu, N., Kartheuser, B., … Jonas, A. M. (2018). Environmentally friendly super-water-repellent fabrics prepared from water-based suspensions. *ACS Applied Materials and Interfaces, 10*(18), 15346–15351. https://doi.org/10.1021/acsami.8b02707

Cathey, A. L., Nguyen, V. K., Colacino, J. A., Woodruff, T. J., Reynolds, P., & Aung, M. T. (2023). Exploratory profiles of phenols, parabens, and per- and poly-fluoroalkyl substances among NHANES study participants in association with previous cancer diagnoses. *Journal of Exposure Science and Environmental Epidemiology.*. https://doi.org/10.1038/s41370-023-00601-6

Chen, D., Chen, F., Zhang, H., Yin, X., & Zhou, Y. (2016). Preparation and characterization of novel hydrophobic cellulose fabrics with polyvinylsilsesquioxane functional coatings. *Cellulose, 23*(1), 941–953. https://doi.org/10.1007/s10570-015-0820-y

Chen, Y., Zhang, X., Wang, B., Lv, M., Zhu, Y., & Gao, J. (2017). Fabrication and characterization of novel shape-stabilized stearic acid composite phase change materials with tannic-acid-templated mesoporous silica nanoparticles for thermal energy storage. *RSC Advances, 7*(26), 15625–15631. https://doi.org/10.1039/c7ra00964j

Cheng, Q. Y., Zhao, X. L., Weng, Y. X., Li, Y. D., & Zeng, J. B. (2019). Fully sustainable, nanoparticle-free, fluorine-free, and robust Superhydrophobic cotton fabric fabricated via an eco-friendly method for efficient oil/water separation. *ACS Sustainable Chemistry and Engineering.*. https://doi.org/10.1021/acssuschemeng.9b03852

Clanet, C., Béguin, C., Richard, D., & Quéré, D. (2004). Maximal deformation of an impacting drop. *Journal of Fluid Mechanics, 517*, 199–208. https://doi.org/10.1017/S0022112004000904

Corazzari, I., Nisticò, R., Turci, F., Faga, M. G., Franzoso, F., Tabasso, S., & Magnacca, G. (2015). Advanced physico-chemical characterization of chitosan by means of TGA coupled on-line with FTIR and GCMS: Thermal degradation and water adsorption capacity. *Polymer Degradation and Stability, 112*, 1–9. https://doi.org/10.1016/j.polymdegradstab. 2014.12.006

Diaz, B. R., & Crick, C. R. (2023). Superhydrophobic coatings with environmentally friendly materials. In J. O. Dr. (Ed.), *Superhydrophobic coating - recent advances in theory and applications*. IntechOpen. https://doi.org/10.5772/intechopen.1002753 (p. Ch. 0).

European Commission. Directorate-General for Justice and Consumers. (2023). *Safer products for all: 2022 results.* doi:978–92–68-00279-7.

Fleetwood, S. K., Bell, S., Jetter, R., & Foster, E. J. (2023). Plant-based, aqueous, water-repellent sprays for coating textiles. *Soft Matter, 19*(36), 7020–7032. https://doi.org/10.1039/d3sm00720k

Forsman, N., Johansson, L. S., Koivula, H., Tuure, M., Kääriäinen, P., & Österberg, M. (2020). Open coating with natural wax particles enables scalable, non-toxic hydrophobation of cellulose-based textiles. *Carbohydrate Polymers, 227*. https://doi.org/10.1016/j.carbpol.2019.115363

Forsman, N., Lozhechnikova, A., Khakalo, A., Johansson, L. S., Vartiainen, J., & Österberg, M. (2017). Layer-by-layer assembled hydrophobic coatings for cellulose nanofibril films and textiles, made of polylysine and natural wax particles. *Carbohydrate Polymers, 173*, 392–402. https://doi.org/10.1016/j.carbpol.2017.06.007

Hou, K., Zeng, Y., Zhou, C., Chen, J., Wen, X., Xu, S., Cheng, J., & Pi, P. (2018). Facile generation of robust POSS-based superhydrophobic fabrics via thiol-ene click chemistry. *Chemical Engineering Journal, 332*, 150–159. https://doi.org/10.1016/j.cej.2017.09.074

Iqbal, Y., Ahmed, I., Irfan, M. F., Chatha, S. A. S., Zubair, M., & Ullah, A. (2023). Recent advances in chitosan-based materials; the synthesis, modifications and biomedical applications. *Carbohydrate Polymers, 321*, Article 121318. https://doi.org/10.1016/j.carbpol.2023.121318

Jing, X., Li, X., Jiang, Y., Zhao, R., Ding, Q., & Han, W. (2021). Excellent coating of collagen fiber/chitosan-based materials that is water- and oil-resistant and fluorine-free. *Carbohydrate Polymers, 266*. https://doi.org/10.1016/j.carbpol.2021.118173

Ladiè, R., Cosentino, C., Tagliaro, I., Antonini, C., Bianchini, G., & Bertini, S. (2021). Supramolecular structuring of hyaluronan-lactose-modified chitosan matrix: Towards high-performance biopolymers with excellent biodegradation. *Biomolecules, 11*(3), 1–19. https://doi.org/10.3390/biom11030389

Lahiri, S. K., Zhang, P., Zhang, C., & Liu, L. (2019). Robust fluorine-free and self-healing Superhydrophobic coatings by H 3 BO 3 incorporation with SiO 2 -alkyl-Silane@ PDMS on cotton fabric. *ACS Applied Materials and Interfaces, 11*(10), 10262–10275. https://doi.org/10.1021/acsami.8b20651

Li, W., & Amirfazli, A. (2005). A thermodynamic approach for determining the contact angle hysteresis for superhydrophobic surfaces. *Journal of Colloid and Interface Science, 292*(1), 195–201. https://doi.org/10.1016/j.jcis.2005.05.062

Mao, T., Kuhn, D. C. S., & Tran, H. (1997). Spread and rebound of liquid droplets upon impact on flat surfaces. *AICHE Journal, 43*(9), 2169–2179. https://doi.org/10.1002/aic.690430903

Mazzon, G., Contardi, M., Quilez-Molina, A., Zahid, M., Zendri, E., Athanassiou, A., & Bayer, I. S. (2021). Antioxidant and hydrophobic cotton fabric resisting accelerated ageing. *Colloids and Surfaces A: Physicochemical and Engineering Aspects, 613*. https://doi.org/10.1016/j.colsurfa.2020.126061

Mohseni, M., Lahiri, S. K., Nadaraja, A. V., Sundararaj, U., & Golovin, K. (2023). Durable and comfortable superoleophobic fabrics utilizing ultra-short-chain fluorinated surface chemistry. *Chemical Engineering Journal, 471*. https://doi.org/10.1016/j.cej.2023.144726

Montero-Martínez, G., & García-García, F. (2016). On the behaviour of raindrop fall speed due to wind. *Quarterly Journal of the Royal Meteorological Society, 142*(698), 2013–2020. https://doi.org/10.1002/qj.2794

Niemczyk, A., Goszczyńska, A., Gołda-Cępa, M., Kotarba, A., Sobolewski, P., & El Fray, M. (2019). Biofunctional catheter coatings based on chitosan-fatty acids derivatives. *Carbohydrate Polymers, 225*. https://doi.org/10.1016/j.carbpol.2019.115263

Nisticò, R., Guerretta, F., Benzi, P., & Magnacca, G. (2020). Chitosan-derived biochars obtained at low pyrolysis temperatures for potential application in electrochemical energy storage devices. *International Journal of Biological Macromolecules, 164*, 1825–1831. https://doi.org/10.1016/j.ijbiomac.2020.08.017

Petroni, S., Tagliaro, I., Antonini, C., D'Arienzo, M., Orsini, S. F., Mano, J. F., Brancato, V., Borges, J., & Cipolla, L. (2023). Chitosan-Based Biomaterials: Insights into Chemistry, Properties, Devices, and Their Biomedical Applications. In *Marine Drugs* (Vol. 21, Issue 3). Multidisciplinary Digital Publishing Institute (MDPI). doi:https://doi.org/10.3390/md21030147.

Porpiglia, N. M., Tagliaro, I., Pellegrini, B., Alessi, A., Tagliaro, F., Russo, L., … Bertini, S. (2024). Chitosan derivatives as dynamic coatings for transferrin glycoform separation in capillary electrophoresis. *International Journal of Biological Macromolecules, 254*. https://doi.org/10.1016/j.ijbiomac.2023.127888

Qi, P., Wang, S., Wang, W., Sun, J., Yuan, H., & Zhang, S. (2022). Chitosan/sodium polyborate based micro-nano coating with high flame retardancy and superhydrophobicity for cotton fabric. *International Journal of Biological Macromolecules, 205*, 261–273. https://doi.org/10.1016/j.ijbiomac.2022.02.062

Raeisi, M., Kazerouni, Y., Mohammadi, A., Hashemi, M., Hejazi, I., Seyfi, J., … Davachi, S. M. (2021). Superhydrophobic cotton fabrics coated by chitosan and titanium dioxide nanoparticles with enhanced antibacterial and UV-protecting properties. *International Journal of Biological Macromolecules, 171*, 158–165. https://doi.org/10.1016/j.ijbiomac.2020.12.220

Rioboo, R., Delattre, B., Duvivier, D., Vaillant, A., & De Coninck, J. (2012). Superhydrophobicity and liquid repellency of solutions on polypropylene. In , *175*. *Advances in Colloid and Interface Science* (pp. 1–10). Elsevier B.V. https://doi.org/10.1016/j.cis.2012.03.003.

Sachan, R., & Purwar, R. (2022). Silica modified candelilla wax/thermoplastic polyurethane blend coatings for hydrophobic textiles. *Journal of the Textile Institute, 113*(7), 1302–1308. https://doi.org/10.1080/00405000.2021.1926128

Sahariah, P., & Másson, M. (2017). Antimicrobial chitosan and chitosan derivatives: A review of the structure-activity relationship. In , *18*. *Biomacromolecules* (pp. 3846–3868). American Chemical Society. https://doi.org/10.1021/acs.biomac.7b01058, 11.

Saji, V. S. (2020). Wax-based artificial superhydrophobic surfaces and coatings. In , *Vol. 602*. *Colloids and surfaces a: Physicochemical and engineering aspects*. Elsevier B.V. https://doi.org/10.1016/j.colsurfa.2020.125132.

Sreekumar, S., Wattjes, J., Niehues, A., Mengoni, T., Mendes, A. C., Morris, E. R., … Moerschbacher, B. M. (2022). Biotechnologically produced chitosans with nonrandom acetylation patterns differ from conventional chitosans in properties and activities. *Nature. Communications, 13*(1). https://doi.org/10.1038/s41467-022-34483-3

Stalder, A. F., Kulik, G., Sage, D., Barbieri, L., & Hoffmann, P. (2006). A snake-based approach to accurate determination of both contact points and contact angles. Colloids and Surfaces A: Physicochemical and Engineering Aspects, 286(1–3), 92–103. doi:https://doi.org/10.1016/j.colsurfa.2006.03.008.

Suryaprabha, T., Ha, H., Hwang, B., & Sethuraman, M. G. (2023). Self-cleaning, superhydrophobic, and antibacterial cotton fabrics with chitosan-based composite coatings. *International Journal of Biological Macromolecules, 250*. https://doi.org/10.1016/j.ijbiomac.2023.126217

Tagliaro, I., Musile, G., Caricato, P., Dorizzi, R. M., Tagliaro, F., & Antonini, C. (2023). Chitosan film sensor for Ammonia detection in microdiffusion analytical devices. *Polymers, 15*(21). https://doi.org/10.3390/polym15214238

Tagliaro, I., Seccia, S., Pellegrini, B., Bertini, S., & Antonini, C. (2023). Chitosan-based coatings with tunable transparency and superhydrophobicity: A solvent-free and

fluorine-free approach by stearoyl derivatization. *Carbohydrate Polymers, 302*. https://doi.org/10.1016/j.carbpol.2022.120424

Vo, D. T., & Lee, C. K. (2017). Cells capture and antimicrobial effect of hydrophobically modified chitosan coating on Escherichia coli. *Carbohydrate Polymers, 164*, 109–117. https://doi.org/10.1016/j.carbpol.2017.01.093

Wu, J., Hu, Z., Lu, W., Yu, L., Wei, H., Yang, X., Zhou, H., Wang, D., Li, W., & Yan, H. (2022). Fabricating self-stratifying coating for superhydrophobic cotton textile. *Journal of Applied Polymer Science, 139*(17). https://doi.org/10.1002/app.52008

Zhang, J., Pei, X., Liu, Y., Ke, X., Peng, Y., Weng, Y., Zhang, Q., & Chen, J. (2023). *Combining Chitosan, Stearic Acid, and (Cu-, Zn-) MOFs to Prepare Robust Superhydrophobic Coatings with Biomedical Multifunctionalities*. Advanced Healthcare Materials. https://doi.org/10.1002/adhm.202300746

Zhang, S., Liao, Y., Lu, K., Wang, Z., Wang, J., Lai, L., Xin, W., Xiao, Y., Xiong, S., & Ding, F. (2023). Chitosan/silica hybrid aerogels with synergistic capability for superior hydrophobicity and mechanical robustness. *Carbohydrate Polymers, 320*. https://doi.org/10.1016/j.carbpol.2023.121245

Zhao, Y., Liu, E., Fan, J., Chen, B., Hu, X., He, Y., & He, C. (2019). Superhydrophobic PDMS/wax coated polyester textiles with self-healing ability via inlaying method. *Progress in Organic Coatings, 132*, 100–107. https://doi.org/10.1016/j.porgcoat.2019.03.043

Zhu, Q., Gao, Q., Guo, Y., Yang, C. Q., & Shen, L. (2011). Modified silica sol coatings for highly hydrophobic cotton and polyester fabrics using a one-step procedure. *Industrial and Engineering Chemistry Research, 50*(10), 5881–5888. https://doi.org/10.1021/ie101825d